Environment International 178 (2023) 108069

Contents lists available at ScienceDirect

Environment International

journal homepage: www.elsevier.com/locate/envint

Full length article

Adjusting elemental carbon emissions in Northeast Asia using observed surface concentrations of downwind area and simulated contributions

Yoon-Hee Kang [a,1], Kyuwon Son [b,1], Byeong-Uk Kim [c], YuWoon Chang [d], Hyun Cheol Kim [f,g], Joshua P. Schwarz [h], Soontae Kim [i,*]

[a] Environmental Research Institute, Ajou University, Suwon, Republic of Korea
[b] Department of Environmental Engineering, Ajou University, Suwon, Republic of Korea
[c] Georgia Environmental Protection Division, Atlanta, GA 30354, United States
[d] Department of Air Quality Research, Climate and Air Quality Research Division, National Institute of Environmental Research, Incheon, Republic of Korea
[f] Cooperative Institute for Satellite Earth System Studies, University of Maryland, MD 20742, United States
[g] Air Resources Laboratory, National Oceanic and Atmospheric Administration, College Park, MD 20740, United States
[h] National Oceanic and Atmospheric Administration Earth System Research Laboratory, Chemical Sciences Laboratory, Boulder, CO 80305, United States
[i] Department of Environmental and Safety Engineering, Ajou University, Suwon, Republic of Korea

ARTICLE INFO

Handling Editor: Xavier Querol

Keywords:
Elemental carbon
Source-receptor relationship
Air quality model
Emission adjustment
Korea-United States Air Quality

ABSTRACT

In this study, we developed a practical approach to augment elemental carbon (EC) emissions to improve the reproducibility of the most recent air quality with photochemical grid modeling in support of source-receptor relationship analysis. We demonstrated the usefulness of this approach with a series of simulations for EC concentrations over Northeast Asia during the 2016 Korea-United States Air Quality study. Considering the difficulty of acquiring EC observational data in foreign countries, our approach takes two steps: (1) augmenting upwind EC emissions based on simulated upwind contributions and observational data at a downwind EC monitor considered as the most representative monitor for upwind influences and (2) adjusting downwind EC emissions based on simulated downwind contributions, including the effects of updated upwind emissions from the first step and observational data at the downwind EC monitors. The emission adjustment approach resulted in EC emissions 2.5 times higher than the original emissions in the modeling domain. The EC concentration in the downwind area was observed to be 1.0 μg m^{-3} during the study period, while the simulated EC concentration was 0.5 μg m^{-3} before the emission adjustment. After the adjustment, the normalized mean error of the daily mean EC concentration decreased from 48 % to 22 % at ground monitor locations. We found that the EC simulation results were improved at high altitudes, and the contribution of the upwind areas was greater than that of the downwind areas for EC concentrations downwind with or without emission adjustment. This implies that collaborating with upwind regions is essential to alleviate high EC concentrations in downwind areas. The developed emission adjustment approach can be used for any upwind or downwind area when transboundary air pollution mitigation is needed because it provides better reproducibility of the most recent air quality through modeling with improved emission data.

Abbreviations: EC, elemental carbon; BC, black carbon; $PM_{2.5}$, particulate matter (diameter <2.5 μm); KORUS-AQ, Korea-United States Air Quality; SRR, source-receptor relationship; REAS, Regional Emission inventory in Asia; CAPSS, Clean Air Policy Support System; MADIS, Meteorological Assimilation Data Ingest System; NAAQMN, National Ambient Air Quality Monitoring Network; WRF, Weather Research and Forecasting; CMAQ, Community Multiscale Air Quality; ISAM, Integrated Source Apportionment Method; RMSE, root mean square error; IOA, index of agreement; NME, normalized mean error; GRGM, generalized reduced gradient method; PMTRX, pseudoinverse matrix; REGF, regression function; PBL, planetary boundary layer.

* Corresponding author.
E-mail address: soontaekim@ajou.ac.kr (S. Kim).
[1] These two authors contributed equally to the paper.

https://doi.org/10.1016/j.envint.2023.108069
Received 27 February 2023; Received in revised form 21 June 2023; Accepted 26 June 2023
Available online 27 June 2023

1. Introduction

Elemental carbon (EC) is a part of $PM_{2.5}$ (particulate matter with an aerodynamic diameter<2.5 μm) that is often referred to as black carbon (BC) (Andreae and Gelencsér, 2006; Petzold et al., 2013). Previous studies have reported that relatively low concentrations of EC are present in the atmosphere, compared to those of other major $PM_{2.5}$ constituents (Cheng et al., 2016; Krall et al., 2013; Qiu et al., 2016). For example, during the Korea-United States Air Quality (KORUS-AQ) campaign period in South Korea, the average EC concentration (1.2 μg m^{-3}) was lower than the average concentrations of secondary inorganic air pollutants such as ammonium (4.9 μg m^{-3}), sulfate (6.7 μg m^{-3}), and nitrate (8.1 μg m^{-3}) (Lee et al., 2020). Furthermore, studies in Northeast Asia over the last two decades have reported that observed and simulated annual average EC concentrations ranged from 0.3 to 5.4 μg m^{-3}, while concentrations of other $PM_{2.5}$ components were much higher than these values (He et al., 2004; Kondo et al., 2006; Park and Cho, 2011; Viana et al., 2007; Wang et al., 2014). However, health studies have indicated that EC poses a higher risk to human health than other $PM_{2.5}$ constituents when an equal amount of air pollutants is inhaled (Bae et al., 2019; IARC, 2016; Janssen et al., 2011; Lee et al., 2017; Morawska et al., 2005; Rappazzo et al., 2015).

As a primary air pollutant with a low reactivity and long residence time in the atmosphere, EC can be transported over long distances across regions (Khan et al., 2006; Shu et al., 2017; Wolff, 1981; Yu et al., 2004). Therefore, to manage this highly adverse air pollutant, it is essential to understand the fate of EC using some analytical approaches such as source-receptor relationship (SRR) analysis (Blanchard et al., 2019; Wagstrom and Pandis, 2011; Yamagami et al., 2019). Previous studies have used three-dimensional photochemical models and observations to estimate the effects of the long-range transport of EC between regions (Aamaas et al., 2011; Kang et al., 2006; Li et al., 2016; Wagstrom and Pandis, 2011; Xing et al., 2020).

An emissions inventory that reflects human activities and natural events is one of the core inputs to three-dimensional photochemical models and, therefore, key information to be used for SRR studies (Fiore et al., 2009; Fowler et al., 2005). However, developing a representative emissions inventory that accurately reflects human activities and natural events is not an easy task, especially in recent years. This is because it takes great effort and time to build a reliable emissions inventory, but emissions change over time along with human activities and natural events. For example, the Regional Emission inventory in ASia (REAS) v3.1, one of the most frequently used and up-to-date emissions inventories for photochemical modeling in Northeast Asia, indicated that BC emissions in China were 3.5×10^5 tons for the most recent inventory year of 2015, which is>3.0×10^5 tons reported for 2010 (Kurokawa and Ohara, 2020). Further, according to the national emissions inventory of South Korea, the Clean Air Policy Support System (CAPSS), the most recent emissions inventory reported that EC emissions were 10 % lower for the most recent inventory year of 2019 than the 1.6×10^4 tons reported for 2016 (NAIR, 2022). As shown by these examples, even the most recent emissions inventories do not necesarrily reflect the rapid changes in real-world emissions as it is inevitable to have a time lag between the years that emissions inventory data represent and the year when a bottom-up emissions inventory is published. This time lag can cause a poor reproducibility of modeled air quality for years more recent than the inventory year due to the difficulty of reflecting changes in emission activities (Frey and Zheng, 2002; Zhao et al., 2011).

To reduce the uncertainties of bottom-up emissions inventories, including the time lag between the model year and the inventory year, many researchers have adopted top-down approaches that reflect the most recent status of air pollution to adjust past emissions contained in emissions inventories with observations, such as those from satellite measurements (Bae et al., 2020; Kim et al., 2014; Stavrakou et al., 2013; Zhang et al., 2018). Other studies have adopted more resource-consuming inverse modeling techniques with observed and simulated data for the entire study area (Hu et al., 2009a; Hu et al., 2009b; Jorquera and Castro, 2010). However, approaches that rely on country-specific EC observational data can be challenging in Northeast Asia because country-specific EC observations are hard to acquire, especially for scientists from outside the region. Nevertheless, it is critical to have emissions inventories as accurate as possible to ensure that observed air pollutant concentrations are reproducible with modeling to support SRR analysis as the credibility of SRR analyses is dependent on the performance of air quality modeling.

In this study, to overcome the restricted access to EC observations for different areas (i.e., country-specific EC observations), we propose a two-step emission adjustment method to improve the reproducibility of EC simulations and demonstrate its utility by using the proposed method to adjust EC emissions over Northeast Asia. First, we utilized modeled region-by-region EC contributions to adjust the EC emissions in upwind regions. As EC has suitable physicochemical characteristics for representing the impact of the emission source (Heintzenberg and Winkler, 1991; Ogren and Charlson, 1984), the EC emissions adjustment over upwind regions where observed EC concentrations were not secured was performed based on a downwind monitoring site that can represent upwind influences. Second, we conducted an observation-based EC emission adjustment to modeling results for the downwind area in South Korea because EC observations in South Korea were relatively easy to acquire for this study. To find an optimal adjustment method, we explored three optimization tools that aim to minimize the differences between observed and modeled EC concentrations. To demonstrate the effectiveness of our approach, we compared the modeled results both with or without the application of the emission adjustment approach developed in this study. Additionally, we compared the changes in regional EC emissions and in upwind/downwind contributions to EC concentrations over South Korea before and after the adjustment. To validate the approach proposed in this study, modeled results with EC emissions before and after the adjustment based on surface observations were compared to airborne measurements during the KORUS-AQ 2016.

2. Materials and methods

2.1. Observation data

Meteorological Assimilation Data Ingest System (MADIS) data were used to evaluate the reproducibility of simulated 10-m wind speeds and 2-m temperatures. We used observed air pollutant concentration data from both the National Ambient Air Quality Monitoring Network (NAAQMN) in China and the South Korean Air Monitoring Stations (AMS) to evaluate simulated $PM_{2.5}$ and 8-h ozone (O_3) at the surface level. We used data from six supersites in South Korea to evaluate the model performance for EC concentrations before and after the EC emission adjustment. These six supersites regularly measure concentrations of individual $PM_{2.5}$ components, including EC. The locations of the meteorological stations and air pollutant monitoring stations that collected the data used in this study are shown in Fig. 1. The EC emissions from upwind areas outside South Korea (e.g., China, North Korea) affect the EC concentrations in South Korea because it is located in the mid-latitude region of the northern hemisphere and is, thus, influenced by westerly winds, as shown in Fig. A1 (Uno et al., 2020; You et al., 2021). Therefore, we defined South Korea as a "downwind area" and foreign regions as "upwind areas" (Fig. 1). Detailed descriptions on the EC observational data and sampling method are provided in Appendix A.

The Baengnyeong supersite (37°57′52.9″ N, 124°38′02.4″ E) is located on Baengnyeong Island in the Yellow Sea, approximately 200 km east of the Shandong Peninsula of China and the northwestern tip of South Korea (NGII, 2022). There are few domestic anthropogenic emission sources in and around the Baengnyeong supersite. Therefore, its observational data are useful for analyzing the effect of the long-range transport of air pollutants (Kim et al., 2021b; Kim, 2000; Lee

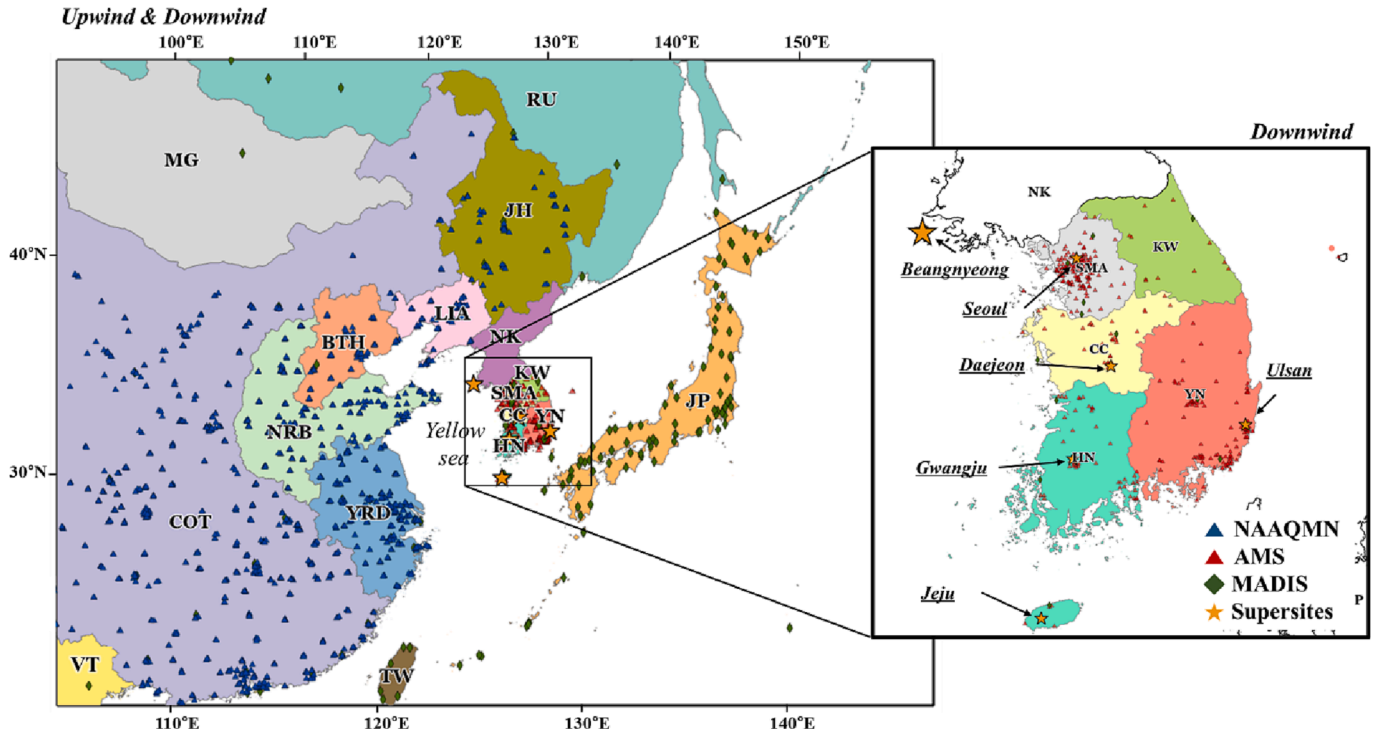

Fig. 1. Maps of upwind and downwind areas in the modeling domain. Locations of South Korean Air Monitoring Stations (AMS) and supersites are depicted with red triangles and orange stars, respectively. Locations of Chinese National Ambient Air Quality Monitoring Network (NAAQMN) stations are denoted with blue triangles. Green diamonds depict the locations of Meteorological Assimilation Data Ingest System (MADIS) sites. The map contains the definition of 17 analysis regions: Beijing–Tianjin–Hebei (BTH), Chungcheong (CC), Other Chinese areas in the domain (COT), Honam (HN), Jilin–Heilongjiang (JH), Japan (JP), Gangwon (KW), Liaoning (LIA), Mongolia (MG), North Korea (NK), Near Beijing (NRB), Russia (RU), Seoul Metropolitan Area (SMA), Taiwan (TW), Vietnam (VT), Yangtze River Delta (YRD), and Youngnam (YN). (For interpretation of the references to colour in this figure legend, the reader is referred to the web version of this article.)

et al., 2015a,2015b; Lee et al., 2019a,2019b; Sung et al., 2017). For this study, we assumed that the Baengnyeong supersite could sufficiently reflect the contribution of major upwind regions to South Korea. We used the Seoul, Gwangju, Daejeon, and Ulsan supersites (located in the inland of South Korea) to adjust EC emissions over the downwind area. The EC concentration at the Jeju supersite was less affected by upwind concentrations than that at the Baengnyeong supersite and had a lower downwind concentration than at other supersites (Lee et al., 2015a,2015b; So et al., 2019). Because the main contributor of EC concentration in the Jeju supersite could not be clearly defined, we only used the data from this supersite to evaluate the model performance.

To evaluate the model performance for EC aloft, we used BC observations over South Korea that were measured using a DC-8 aircraft. To compare our simulated EC concentrations with aircraft observational data (averaged at 60-s intervals), we interpolated simulated EC concentrations at 1-h intervals and assumed a linear change over time. The BC observations with the DC-8 aircraft only included the concentrations of particles with diameters ranging 100–550 nm. In CMAQ simulations, particles are divided into three modes—Aiken, accumulation, and coarse modes—according to their size (Binkowski and Roselle, 2003; Binkowski, 1999). The fraction of each mode was considered when the simulated concentrations of aerosol were calculated (EPA, accessed on May 16, 2022). The mean and standard deviation of simulated EC particle diameters in the accumulation mode were 0.21 μm and 1.80 μm, respectively. In this study, to consider the diameter of EC particles in the accumulation mode, only 36 % of the simulated EC concentrations (i.e., the percentage of particles in the accumulation mode over all particles) were used for a comparison with the aircraft-measured BC concentrations. The comparison considered the modal particle size distribution adopted by Ensberg et al. (2013). We selected specific days to compare aircraft-measured and simulated EC concentrations by considering the effect of upwind and downwind emissions. May 17–18, 2016 and May 25 and 27, 2016 were selected as representative days with a strong influence of upwind and downwind emissions in South Korea, respectively (NIER, 2017; Cho et al., 2021; Choi et al., 2019; Crawford et al., 2021; Kim et al., 2021a).

2.2. Air quality simulation

Meteorological modeling was performed using Weather Research and Forecasting (WRF) version 3.9.1 (Skamarock and Klemp, 2008). We used Final Operational Global Analysis data as the initial conditions for the WRF simulation (NCEP, 2000) and processed the simulation results using Meteorology-Chemistry Interface Processor version 4.3 to generate input data for the Community Multiscale Air Quality model (CMAQ). Natural emissions from the Northeast Asia region were determined using the Model of Emissions of Gases and Aerosols from Nature (MEGAN) version 2.04. For anthropogenic emissions, we considered the spatio-temporal and chemical characteristics in emission processing with the Sparse Matrix Operator Kernel Emission version 3.1 (Houyoux et al., 2000). We used CAPSS 2016 for anthropogenic emissions over South Korea, while KORUS v5 was used for anthropogenic emissions over Northeast Asia excluding South Korea (Choi et al., 2020; Jang et al., 2020).

CMAQ version 5.3.2 was selected as the three-dimensional photochemical grid model for the air quality simulation in this study (Appel et al., 2021; Byun and Schere, 2006). The simulation domain included South Korea, China, and Japan (Fig. 1), and the horizontal grid resolution of the modeling domain was 27 km. For the air quality simulation, SAPRC07 and AERO6 were utilized as the gas-phase chemical mechanism and the aerosol module, respectively (Binkowski and Roselle, 2003; Carter, 2010). The meteorological and air quality simulation period was set from April 1 to May 31, 2016 to ensure a sufficient spin-up time because the KORUS-AQ period (defined as May 2016 in this

study) was used as the study period for analysis. The detailed configurations of WRF and CMAQ are shown in Table B1.

The integrated source apportionment method (ISAM) is a tagging method used to quantify the contributions of emission sources within SRR analyses (Environment Protection Agency, 2021). We used the ISAM of CMAQ to quantify the contribution of each region to EC emissions. For ISAM, the six supersites in South Korea were set as receptors for contribution analyses. We defined contributions that originated from the downwind area as "downwind contribution" and contributions that originated from the upwind area as "upwind contribution." We defined the upwind/downwind contribution rate as the percentage of the upwind/downwind contribution to the simulated EC concentration (i.e., the total contribution from all sources). In previous studies, the contribution rate was used to show the relative contribution of a source to the total EC concentration at a receptor area (Chen et al., 2015; Cheng et al., 2021; Lan et al., 2018; Lu et al., 2019; Zhang et al., 2019).

2.3. Model performance evaluation

For model performance evaluation of the meteorological simulation, we used the root mean square error (RMSE) and the index of agreement (IOA) as indicators of agreenment between the observed and simulated data at the MADIS sites. The IOA is one of the performance benchmark indices for the meteorological model used by Emery et al. (2001), who also introduced the normalized mean error (NME) and correlation coefficient (r) as benchmark indices for the air quality model. For model performance evaluation of the air quality simulations, we calculated the RMSE, r, and NME of $PM_{2.5}$ and 8-h O_3 concentrations at the monitors of Chinese NAAQMN and South Korean AMS. Finally, we used the NME and normalized mean bias (NMB) to quantify the effect of the EC emission adjustment method on the model performance for EC concentrations at the six supersites in South Korea. The detailed descriptions and benchmark values of the performance statistics that we used in this study have been previously discussed by Emery et al. (2001, 2017). We evaluated the simulated aloft EC concentrations with the aircraft measurements before and after EC emission adjustment, as described in Section 2.1.

2.4. Emission adjustment method

The first step of our proposed emission adjustment approach required the quantification of the EC contribution of upwind areas to a downwind monitoring site that can represent the influence of the upwind area. To quantify the contributions of EC emissions over Northeast Asia, we used CMAQ-ISAM with 17 regions (12 upwind regions and 5 downwind regions) for tagging in this study. These are shown in Fig. 1 based on administrative boundaries and locations/availability of the supersites.

If we assume that the observed EC concentration at a downwind region is equal to the sum of EC concentrations contributed by upwind and downwind EC emissions, the source-receptor relationship can be expressed as a matrix of equation (1), as shown in Fig. 2. Then, this matrix of equations can be used to find an optimal solution for a monthly regional EC emission adjustment factor to minimize observation–model differences. The multiplication of matrix A (i.e, regional EC contributions) and vector X (i.e., adjustment factors for EC emission sources) result in vector B, which contains the difference between the observed EC concentration and the residual term. In Fig. 2, i is the index of supersites and m is the number of supersites used at each emission adjustment step. Note that m is 1 in the first step because the Baengnyeong supersite that can explicitly address the upwind contribution was the only supersite used, while the second step in the emission adjustment uses 4 supersites (i.e., the Seoul, Deajeon, Gwangju, and Ulsan supersites), where EC concentrations are determined from both

$$A \cdot X = B \qquad (1)$$

Column: the number of adjusting emission source regions (n)

Row: the number of days of the month (31) × the number of sites (m)

A: the number of adjusting emission source regions (n) × 1

X: 1 × 1

B: the number of days of the month (31) × the number of sites (m) × 1

$$\begin{bmatrix} C^{j_1}_{0501,i1} & C^{j_2}_{0501,i1} & C^{j_3}_{0501,i1} & \cdots & C^{j_{n-2}}_{0501,i1} & C^{j_{n-1}}_{0501,i1} & C^{j_n}_{0501,i1} \\ & & \cdots & & & & \\ C^{j_1}_{0531,i1} & C^{j_2}_{0531,i1} & C^{j_3}_{0531,i1} & \cdots & C^{j_{n-2}}_{0531,i1} & C^{j_{n-1}}_{0531,i1} & C^{j_n}_{0531,i1} \\ & & \cdots & & & & \\ & & \cdots & & & & \\ C^{j_1}_{0501,im} & C^{j_2}_{0501,im} & C^{j_3}_{0501,im} & \cdots & C^{j_{n-2}}_{0501,im} & C^{j_{n-1}}_{0501,im} & C^{j_n}_{0501,im} \\ & & \cdots & & & & \\ C^{j_1}_{0531,im} & C^{j_2}_{0531,im} & C^{j_3}_{0531,im} & \cdots & C^{j_{n-2}}_{0531,im} & C^{j_{n-1}}_{0531,im} & C^{j_n}_{0531,im} \end{bmatrix} \cdot \begin{bmatrix} F^{j1}_{05} \\ F^{j2}_{05} \\ F^{j3}_{05} \\ \cdots \\ F^{jn-2}_{05} \\ F^{jn-1}_{05} \\ F^{jn}_{05} \end{bmatrix} = \begin{bmatrix} OBS_{0501,i1} - \varepsilon_{0501,i1} \\ \cdots \\ OBS_{0531,i1} - \varepsilon_{0531,i1} \\ \cdots \\ \cdots \\ OBS_{0501,im} - \varepsilon_{0501,im} \\ \cdots \\ OBS_{0531,im} - \varepsilon_{0531,im} \end{bmatrix}$$

$$\varepsilon_{mmdd,i_m} = \mathrm{MOD}_{mmdd,i_m} - \sum_{j=1}^{n} C^{j_n}_{mmdd,i_m} \qquad (2)$$

Fig. 2. (1) System of equations used to derive the adjusting factors (F^j_{mm}) for regional elemental carbon (EC) emissions based on the modeled contributions ($C^j_{mmdd,i}$) from CMAQ-ISAM simulations and observed EC concentrations ($OBS_{mmdd,i}$). Twelve emission source regions (n) in the upwing regions and one site (m), the Baengnyeong supersite, were used during the first step of the emission adjustment, i.e., $n = 12$ and $m = 1$. In the second step of emission adjustment, five emission source regions in the downwind area and four supersites (the Seoul, Deajeon, Gwangju, and Ulsan supersites) were used, i.e., $n = 5$ and $m = 4$. (2) The residual term ($\varepsilon_{mmdd,i}$) accounts for the difference between the modeled concentrations from the base simulation (MOD_{mmdd,i_m}) and the sum of the contributions ($C^{j_n}_{mmdd,i_m}$) for emission source regions on day dd of month mm at supersite i_m.

upwind and downwind contributions. *j* is the index of emission source regions and *n* is the number of emission source regions at each emission adjustment step (i.e., 12 to account for the upwind regions in the first step and 5 for downwind regions in the second step). *mmdd* represents a given day (*dd*) of a the month (*mm*). $OBS_{mmdd,i}$ is the daily mean observed EC concentration on *mmdd* at supersite *i*. $C^{j}_{mmdd,i}$ is the daily mean EC contribution from the emissions from region *j* on *mmdd* at supersite *i*. F^{j}_{mm} is the monthly EC emission adjustment factor on *mm* for the source region *j*. As indicated in equation (2) in Fig. 2, $\varepsilon_{mmdd,\,i}$ represents the residual term, which accounts for the contributions of the initial condition, boundary condition, and emissions from other regions beyond the 17 emission source regions defined for the CMAQ-ISAM simulation on day *dd* of month *mm* at supersite *i*.

Three optimization methods were tested to solve the matrix to derive adjustment factors: the generalized reduced gradient method (GRGM), pseudoinverse matrix (PMTRX), and regression function (REGF). GRGM assumes a non-linear relationship between the contributions and the adjustment factors by region, while PMTRX and REGF assume a linear relationship. We applied GRGM because a non-linear relationship between EC contribution and emission adjustment factors can exist because the air pollutant concentration is determined not only by emissions but also various conditions, including meteorology and atmospheric processes such as depositions. GRGM has been used to solve non-linear problems in previous studies (Chai et al., 2015; Geem and Geem, 2007; Kim et al., 2007). We utilized the GRGM solver that is named as "GRG Nonlinear" available in Microsoft Excel. The GRGM solver calculates an optimal (maximum or minimum) value for a formula in an objective cell (Dauda et al., 2022). In this study, adjustment factors were calculated to minimize the difference between the observed and calculated EC concentrations using the solver.

Simultaneously, EC also shows a strong linear relationship between concentration and emission because it is a primary air pollutant (Fisher and Sokhi, 2000; Kiesewetter et al., 2013; Kim et al., 2020). Thus, we evaluated PMTRX and REGF, which have been used in previous studies to solve the linear objective function and minimize errors (Cho et al., 2008; Kublanovskaya, 1966; Matveev, 1974; Shu and Lam, 2011). To derive the emission adjustment factor by region (defined as vector X in Fig. 2) in PMTRX, we multiplied both sides of the equation in Fig. 2 with the transposed matrix of A (i.e., A^{t}). Subsequently, the product of A and A^{t} was multiplied with the pseudo inversion matrix. The detailed solving process of deriving a solution through the PMTRX is shown in Appendix C (Fig. C1). In REGF, we used the "regress" function in the Interactive Data Language program (L3HARRIS, accessed on April 6, 2022). We adopted an additional post-processing for REGF results as we expected that EC concentrations adjusted by REGF would be lower than the observed concentrations, while correlation coefficients seemed to be reasonable (not shown here). In the post-processing step, we multiplied the regional adjustment factors with the ratio of the observed and expected EC concentrations that was estimated with REGF to minimize the mean error. Appendix C provides the detailed process used for the REGF (Fig. C2).

We employed three methods for solving the matrix within the two-step emission adjustment for upwind and downwind regions. The first step (i.e., upwind emission adjustment) was performed over EC emissions from 12 upwind regions. As described in Section 2.1, the EC observation at the Baengnyeong supersite represents the foreign impact (Jo et al., 2020; Lee et al., 2015a,2015b). The second step (i.e., downwind emission adjustment) was performed for the modeling result obtained after using upwind EC emissions that were adjusted in the first step. The objective functions for the Seoul, Daejeon, Gwangju, and Ulsan supersites were solved simultaneously to adjust the EC emissions of the downwind regions. Fig. 3 shows the schematic of the two-step EC emission adjustment.

Previous studies have applied the method of estimating the uncertainty of upwind contribution based on a simulation uncertainty at the Baengnyeong supersite (Bae et al., 2021; Kim et al., 2021c). These studies adopted a two-step adjustment for contributions but did not provide regional emission adjustments. In this study, we combined a foreign contribution adjustment using the Baengnyeong supersite and a domestic contribution adjustment at the four inland supersites as a two-step approach for adjusting EC emissions.

3. Results and discussion

3.1. Model performance evaluation for the base simulation

3.1.1. Meteorological model performance

Table 1 shows the results of model performance evaluation for 10-m wind speeds and 2-m temperatures at the MADIS sites located in China (33 sites) and South Korea (26 sites) in May 2016. For the MADIS sites in China, the RMSEs for wind speeds and temperatures were 0.20 m s^{-1} and 0.51 °C, respectively while the IOAs were > 0.9 for both. For the

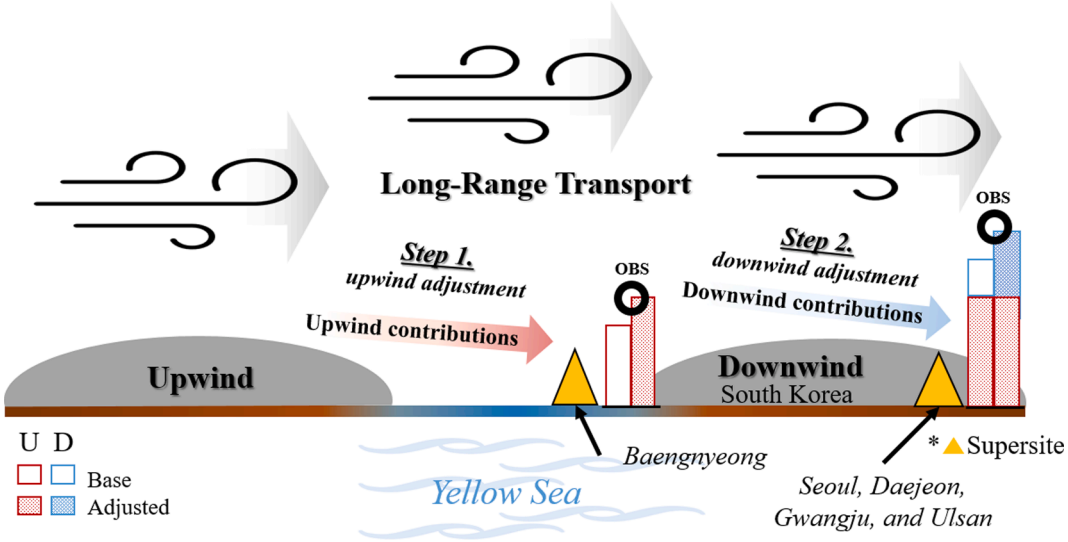

Fig. 3. Illustration of the two-step adjustment approach used in this study for emissions of elemental carbon (EC). Red ("U") and blue ("D") bars represent simulated upwind and downwind contributions, respectively. Hashed bars depict simulated contributions with EC emission adjustment. "OBS" (black circle) denotes observed EC concentrations. (For interpretation of the references to colour in this figure legend, the reader is referred to the web version of this article.)

Table 1
Model performance statistics for 10-m wind speeds and 2-m temperatures at MADIS sites in China and South Korea during May 2016.

Region	Variable	Observed mean	Simulated mean	RMSE	IOA
China	10-m wind speed	3.27 m s^{-1}	3.30 m s^{-1}	0.20 m s^{-1}	0.96
	2-m temperature	20.67 °C	20.60 °C	0.51 °C	0.97
South Korea	10-m wind speed	2.77 m s^{-1}	3.10 m s^{-1}	0.59 m s^{-1}	0.95
	2-m temperature	16.24 °C	17.33 °C	1.11 °C	0.92

Performance goals for 10-m wind speeds by Emery et al. (2001): RMSE $\leq$ 2 m s^{-1} and IOA $\geq$ 0.6. Performance goals for 2-m temperatures by Emery et al. (2001): IOA $\geq$ 0.7. The number of MADIS sites in China and South Korea are 33 and 26, respectively.

MADIS sites in South Korea, the RMSEs for 10-m wind speeds and 2-m temperatures were 0.59 m s^{-1} and 1.11 °C, respectively. The IOAs for both meteorological variables were > 0.9. These performance statistics indicate that meteorological model performance met the performance goal proposed by Emery et al. (2001).

3.1.2. Air quality model performance

The observed monthly mean EC concentrations at each supersite ranged from 0.6 to 1.3 μg m^{-3}. The RMSEs and correlation coefficients at each supersite ranged from 0.2 to 0.8 μg m^{-3} and 0.3–0.9, respectively while the NMEs ranged between 30 % and 62 %. For NMEs, while all sites met the air quality model performance criteria (<75 %) proposed by Emery et al. (2017), four out of the six sites did not meet the performance goal (<50 %) (Table 2). It is worth noting that the meteorological model performance met its benchmark goal, while the simulated EC concentration did not meet the performance criteria entirely. This implies that the EC emission inputs used in the present study had more uncertainty than the meteorological inputs.

The correlation coefficients between the observed and simulated concentrations for the daily mean $PM_{2.5}$ and 8-h O_3 in China at the NAAQMN sites for May 2016 were 0.59 and 0.71 while the NMEs were 21.0 % and 22.2 %, respectively. For South Korea, the correlation coefficients and NMEs for $PM_{2.5}$ concentrations at air monitoring stations (AMS) sites were 0.86 and 28.9 % while those for 8-h O_3 concentration were 0.84 % and 8.2 %, respectively, as shown in Appendix B (Fig. B1). The simulated $PM_{2.5}$ and 8-h O_3 concentrations in this study satisfied the performance goals proposed by Emery et al. (2017).

Table 2
Model performance statistics for elemental carbon (EC) concentrations at each supersite in South Korea during May 2016.

Sites	Observed mean (μg m^{-3})	Simulated mean (μg m^{-3})	RMSE (μg m^{-3})	R	NME (%)
Baengnyeong	1.04	0.42	0.73	0.59	60.06
Seoul	1.32	0.84	0.74	0.36	42.10
Daejeon	1.24	0.55	0.78	0.78	55.95
Gwangju	1.07	0.51	0.64	0.85	52.32
Jeju	1.07	0.41	0.75	0.33	62.22
Ulsan	0.64	0.52	0.21	0.80	26.31

RMSE (root mean square error), *r* (correlation coefficient), NME (normalized mean error).
Performance goals for 24 h EC by Emery et al. (2017): NME $\leq \pm$50 %.
Performance criteria for 24 h EC by Emery et al. (2017): NME $\leq \pm$75 %.

3.2. Results of EC emission adjustment

3.2.1. Upwind emission adjustment

In May 2016, the monthly mean observed and simulated (without adjustment) EC concentrations at the Baengnyeong supersite were 1.0 and 0.4 μg m^{-3}, respectively. After the first step of EC emission adjustment, the monthly mean simulated EC concentrations at the Baengnyeong supersite were 0.9 μg m^{-3} by GRGM, 0.9 μg m^{-3} by REGF, and 1.1 μg m^{-3} by PMTRX. The RMSE of the daily mean simulated EC concentration without adjustment was 0.7 μg m^{-3}. This was reduced to 0.5 μg m^{-3} by GRGM, 0.5 μg m^{-3} by REGF, and 0.6 μg m^{-3} by PMTRX. The NME of the daily mean simulated EC concentration decreased from 60 % before adjustment to 37 % by GRGM, 37 % by REGF, and 50 % by PMTRX. Our results demonstrate that among the three methods that we tested, PMTRX provided the greatest improvement in the monthly mean error but the smallest improvements to RMSE and NME. PMTRX revealed its shortcomings when improving simulated concentrations on a smaller time scale (i.e., daily or hourly) than the emission adjustment time scale (monthly). Further, the correlation coefficient was 0.59 by REGF, matching that of the base simulation, while it decreased to 0.05 by GRGM and 0.11 by PMTRX (Fig. 4). The simulated EC concentrations after emission adjustment for May 22–26 were underestimated compared with the observed concentrations regardless of the emission adjustment method used. Lamb et al. (2018) reported that the EC concentration temporarily increased because of wildfires in Siberia during the period. As this study derived the adjustment factors for upwind regions considering the upwind contribution and observation concentration for the entire adjustment period, the effect of emission adjustment may be limited if the EC concentration changes rapidly because of uninventoried natural events such as wildfires.

We adjusted the EC emissions of the upwind area based on our contribution analysis at the Baengnyeong supersite (as described in Section 2). The effect of the upwind emission adjustment propagated to other supersites in the downwind area. After the first step of EC emission adjustment, the underestimation of the average EC concentration at all supersites in South Korea was mitigated by 0.4–0.5 μg m^{-3} (40–50 %) except at the Ulsan supersite (Fig. B2). The Ulsan supersite had the lowest correlation coefficient (−0.22) for the upwind contribution rate among the six supersites in South Korea. As the Baengnyeong and Ulsan supersites had distinct characteristics in the upwind contribution rate, the improvement on EC simulation uncertainty after adjusting the upwind EC emission may have been limited at the Ulsan supersite.

3.2.2. Downward emission adjustment

The monthly mean EC concentrations averaged over all supersites ranged from 1.0 to 1.2 μg m^{-3} upon the completion of the two-step EC emission adjustment by each method. Compared with the EC concentration before the emission adjustment (0.5 μg m^{-3}), the results from the simulations with adjusted emissions showed that the mean error decreased between observed EC concentration (1.0 μg m^{-3}) and simulated EC concentrations (Fig. 5). The RMSEs for the daily mean EC concentration averaged over all supersites improved in the order of REGF (0.26 μg m^{-3}), GRGM (0.28 μg m^{-3}), and PMTRX (0.33 μg m^{-3}) and decreased to approximately half of that in the simulation before the emission adjustment (0.57 μg m^{-3}). After the emission adjustment, the NMEs for EC concentrations averaged over all supersites improved as follows: 22.2 % by REGF, 22.8 % by GRGM, and 24.5 % by PMTRX. The correlation coefficients were as follows: 0.79 for REGF, 0.69 for GRGM, and 0.61 for PMTRX. A prominent difference in the improvement of the simulated EC concentration for each method could be driven by the difference in EC emissions after adjustment. We found that REGF was deemed to be the optimal method for EC emission adjustment in Northeast Asia in terms of the NME, correlation coefficient, and RMSE. The performance statistics at each supersite when we used REGF are summarized in Table B2.

After the second step of EC emission adjustment, the NMEs at

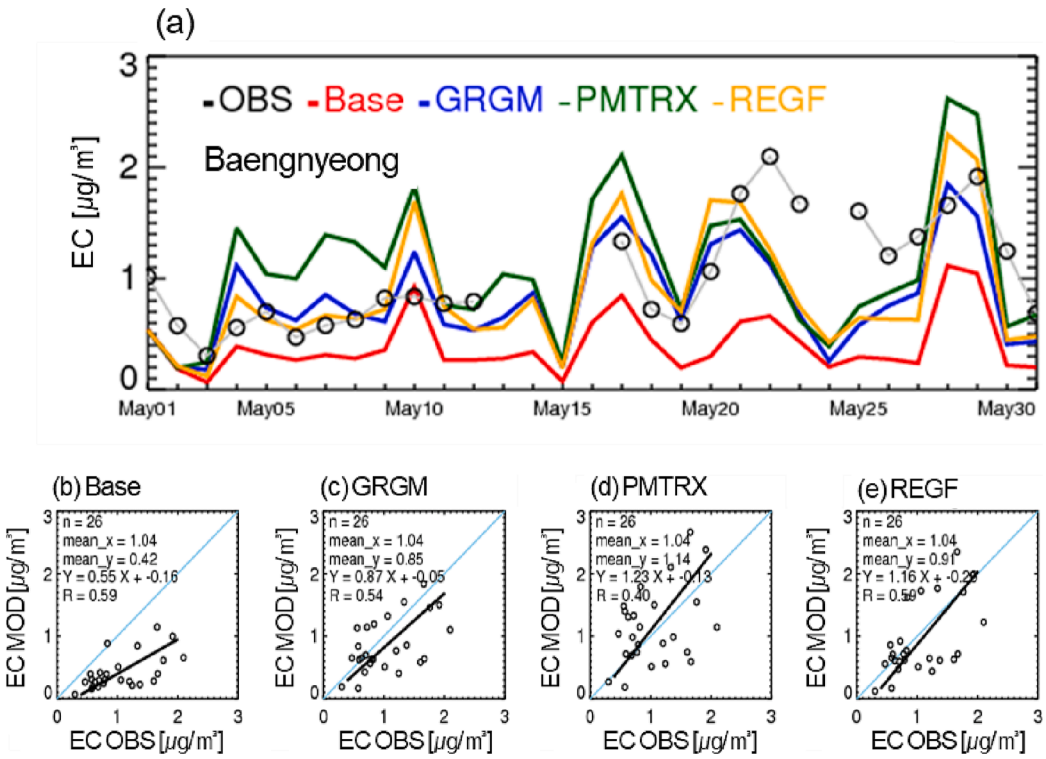

Fig. 4. (a) Time series plot and (b-e) scatter plots of the observed and simulated daily mean elemental carbon (EC) concentrations after the first step of EC emission adjustment at the Baengnyeong supersite in South Korea during May 2016. Legend labels in the time series plot and plot titles of the scatter plots indicate the source of EC concentration data used in each plot: observations ("OBS"), base case simulation ("Base"), and simulations based on adjusted EC emissions using the generalized reduced gradient method ("GRGM"), pseudoinverse matrix ("PMTRX"), and regression function ("REGF").

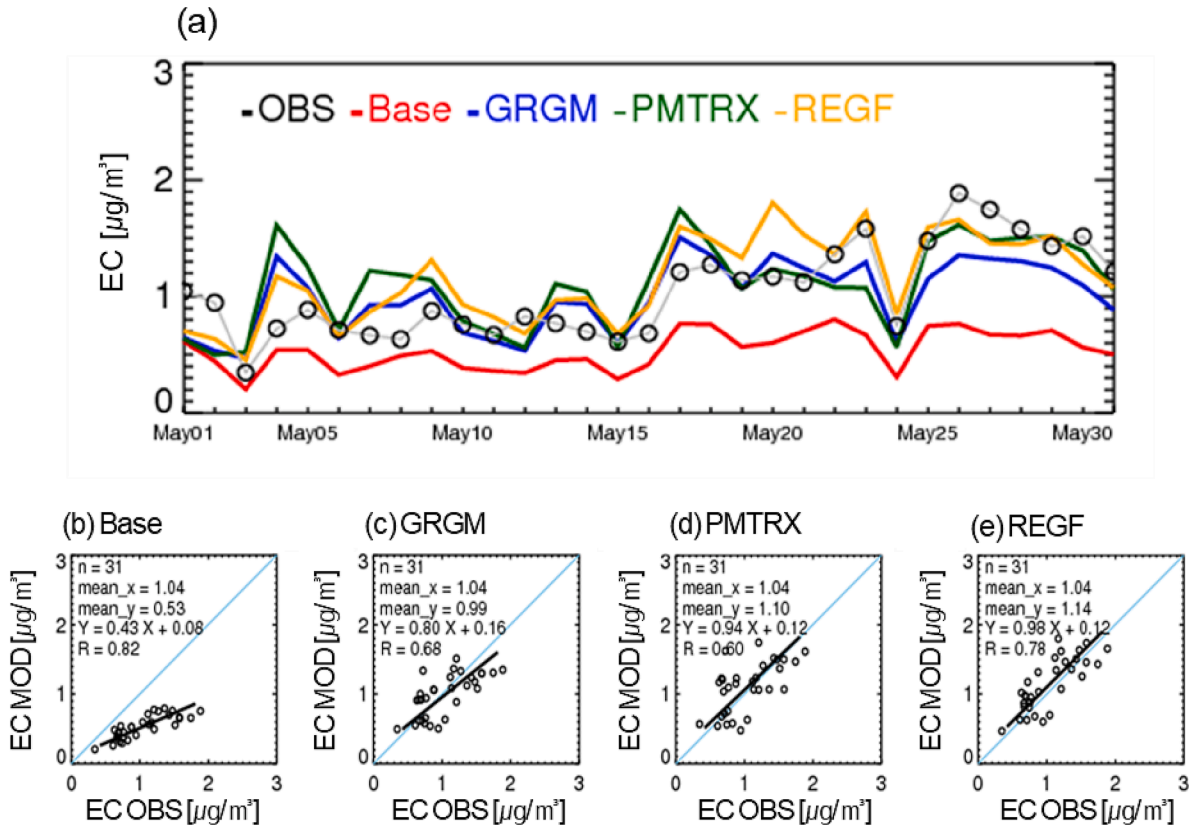

Fig. 5. (a) Time series plot and (b-e) scatter plots of the observed and simulated daily mean elemental carbon (EC) concentrations upon the completion of the second step of EC emission adjustment as average values across all supersites in South Korea during May 2016. Legend labels in the time series plot and plot titles of the scatter plots indicate the source of EC concentration data used in each plot: observations ("OBS"), base case simulation ("Base"), and simulations based on adjusted EC emissions using the generalized reduced gradient method ("GRGM"), pseudoinverse matrix ("PMTRX"), and regression function ("REGF").

supersites improved by 10–30 % compared with those in the simulation before the emission adjustment, except at the Ulsan supersite. Before the emission adjustment, the NMEs at the Baengnyeong, Daejeon, Gwangju, and Jeju supersites did not meet the performance goal proposed by Emery et al. (2017). After EC emission adjustments, the NMEs at these supersites were < 50 %, indicating that the developed method accomplishes sufficient performance improvement to satisfy the performance goal (Fig. B3). When compared with the NME of the simulation before the emission adjustment, the NMEs at the Ulsan supersite degraded by 5 % with GRGM and 39 % with REGF. At the Ulsan supersite, the observed monthly mean EC concentration of 0.6 μg m^{-3} was approximately half of the average EC concentration (1.1 μg m^{-3}) at the other five supersites before the emission adjustment. Unlike other supersites, the simulated EC concentration at the Ulsan supersite was overestimated after the first EC emission adjustment. To minimize underestimation, the second EC emission adjustment was performed simultaneously at all supersites.

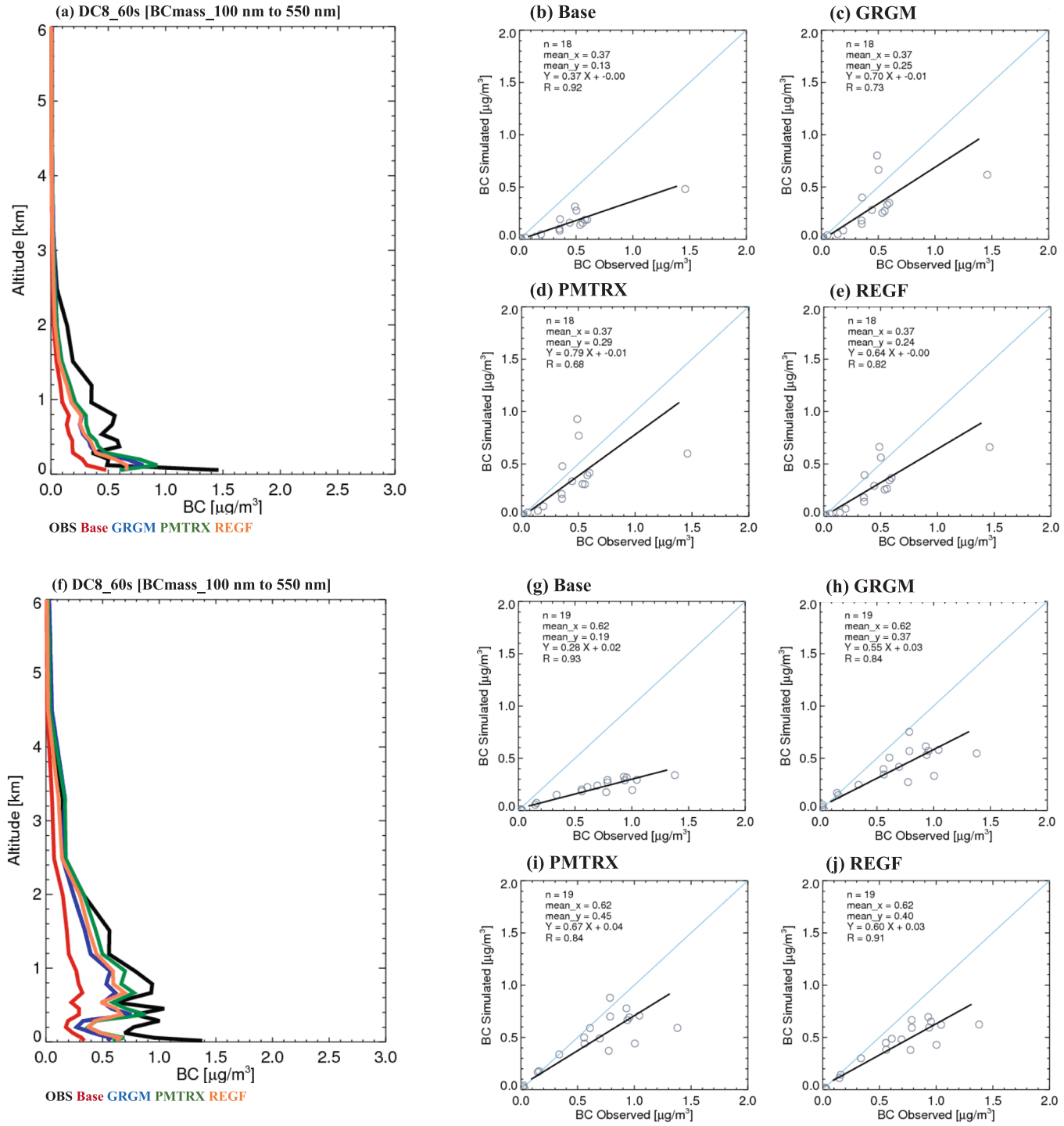

Fig. 6. Vertical profiles and scatter plots for black carbon (BC) concentrations measured by the DC-8 aircraft on (a) May 17 and 18, 2016 and (f) May 25 and 27, 2016. (b–e, g–j) Scatter plot data represent daily averaged BC concentrations. Legend labels and plot titles indicate the source of EC concentration data used in each plot: observations ("OBS"), base case simulation ("Base"), and simulations based on adjusted EC emissions using the generalized reduced gradient method ("GRGM"), pseudoinverse matrix ("PMTRX"), and regression function ("REGF").

Therefore, the reproducibility improvement of simulations for EC concentrations at the Ulsan supersite may have been limited.

3.2.3. EC concentrations aloft after emission adjustment

May 17 and 18, 2016 reportedly showed relatively high effects of downwind emissions on air quality in South Korea during the KORUS-AQ 2016 period (Lamb et al., 2018; Peterson et al., 2019). The mean BC concentration from aircraft measurement for those days was 0.4 μg m^{-3}, while the simulation before the emission adjustment underestimated this value by 0.1 μg m^{-3}. After the two-step EC emission adjustment, the mean simulated EC concentrations for this period were 0.2 μg m^{-3} by REGF, 0.3 μg m^{-3} by GRGM, and 0.3 μg m^{-3} by PMTRX, as shown in Fig. 6(a). In particular, the differences in the simulated EC concentrations before and after the EC emission adjustment were noticeable at altitudes < 2.5 km. Additionally, the closer the aircraft was to the surface, the bigger the difference of EC concentrations before and after the EC emission adjustment was. As downwind emissions were the main factor determining air quality of South Korea during this period, the effect of the adjusted EC emission was primarily observed in lower layers.

On May 25 and 27, 2016, the effect of upwind emissions on air quality in South Korea was relatively high (Tang et al., 2019; Travis et al., 2022; Yu et al., 2020). The mean BC concentration measured by aircraft for those days was 0.6 μg m^{-3}. The mean simulated EC concentration was 0.2 μg m^{-3} in the simulation before the emission adjustment. After the two-step EC emission adjustment, the simulated EC concentrations ranged from 0.4 μg m^{-3} (GRGM) to 0.5 μg m^{-3} (PMTRX), as shown in Fig. 6(b). Unlike May 17 and 18, 2016, the difference in the simulated EC concentrations before and after the EC emission adjustment was remarkable within an altitude of 3.5 km, which is higher than the altitude identified on May 17 and 18, 2016 (i.e., 2.5 km). This result was attributed to a combination of long-range transport effects originating from the adjusted upwind EC emission and the impact of adjusted downwind EC emission. The vertical mixing and long-range transport path of air pollutants could vary according to the mechanical options used in a meteorological model, such as the planetary boundary layer (PBL) scheme (Chatani et al., 2014; Jeong and Kim, 2021; Lee et al., 2019a,2019b; Mao et al., 2006; Moon et al., 2011). Our results indicate that future studies should adjust regional EC emissions considering the PBL scheme and analyze the impact of long-range transport accordingly.

3.3. Comparison of EC adjusted emissions

In this study, the EC emissions from Northeast Asia in May 2016, representing a sum of EC emissions (percentages of the domain wide total emissions) were 6.9 × 10^4 tons: 6.5 × 10^4 tons (94 %) from China, and 0.08 × 10^4 tons (1 %) from South Korea. The highest adjusted EC emission was obtained with the GRGM (3.9 × 10^5 tons), followed by that with PMTRX (3.4 × 10^5 tons) and REGF (1.7 × 10^5 tons) (Fig. 7). After the adjustment, EC emissions increased 2.5–5.7 times compared with the original EC emissions depending on the adjustment method used. The EC emissions adjusted with REGF (the optimal adjustment method identified in this study) increased from the original EC emissions in all regions (Fig. 7). These results imply that the EC emissions in the emissions inventory over Northeast Asia have been significantly underestimated.

The underprediction of EC concentrations owing to the uncertainty of EC emissions over Asia has been reported in previous studies. Wang et al. (2016a,2016b) showed that the inverse modeled EC emissions over China were approximately 1.8 times those of a bottom-up emissions inventory and that the use of the inverse modeled EC emissions improved the accuracy of daily model simulations. Luo et al. (2023) reported that the uncertainty of EC emissions was still large (±221.68 %) after estimating EC emissions inversely as there is no direct EC observation in Beijing-Tianjin-Hebei. In Japan, simulated EC concentrations were underestimated because of a problem of boundary conditions resulting from the underestimation of EC emissions in upwind areas (Chatani et al., 2018).

While the total EC emissions of upwind and downwind areas in the modeling domain increased to 5.7 times the original emissions after adjustment, the increase in EC concentrations in South Korea was much lower, only 2.0 times the EC concentration before the emission adjustment. This may be because the contribution of each emission region to the EC concentration in South Korea varied by region. For instance, the region referred to as “Rest of China” that included LIA, JH, and COT had the greatest EC emission increase regardless of the adjustment method, while contribution of that region to the EC concentration at the Baengnyeong supersite was < 10 % (0.04 μg m^{-3}). This is explained by the emission-to-contribution relationship generally being inversely proportional to the distance between the source and receptor area (Rissman et al., 2013; Su et al., 2018). This implies a necessity for further studies to develop a new method based on observations in source regions for a more accurate adjustment of their emissions.

3.4. Upwind and downwind EC contributions

The upwind and downwind EC contributions were estimated with emissions adjusted with REGF, and their results were compared with those of the simulations before the emission adjustment at the six

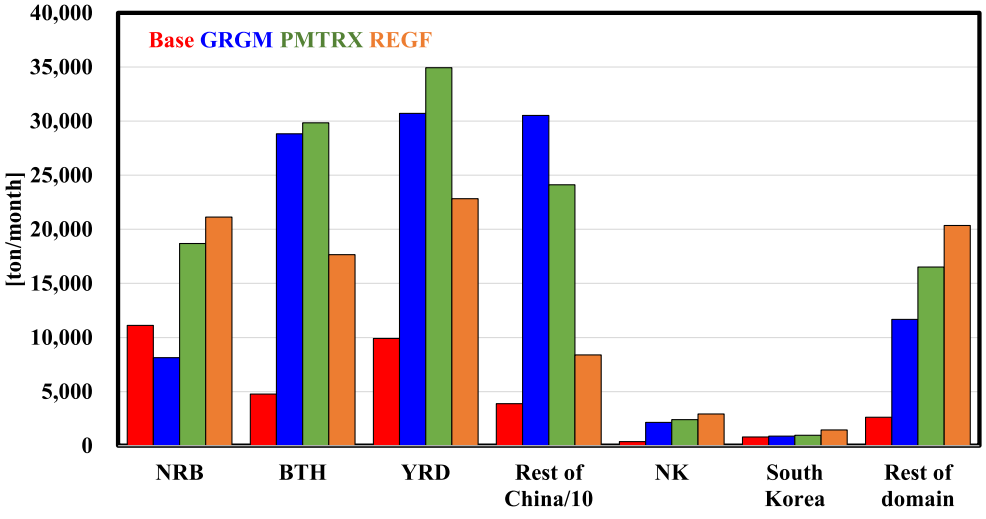

Fig. 7. Monthly elemental carbon emissions from selected regions in Northeast Asia for May 2016. NRB, BTH, YRD, and NK represent emissions from the corresponding areas defined in Fig. 1. “Rest of China” represents emissions from LIA, JH, and COT in Fig. 1. Note that the emissions from ‘Rest of China” were scaled with 1/10. “South Korea” represents emissions from SMA, CC, HN, YN, and KW in Fig. 1. “Rest of domain” represents emissions from JP, TW, MG, RU, and VT in Fig. 1. Legend labels indicate the source of EC concentration data: base case simulation (“Base”) and simulations based on adjusted EC emissions using the generalized reduced gradient method (“GRGM”), pseudoinverse matrix (“PMTRX”), and regression function (“REGF”).

supersites in South Korea. For May 2016, the monthly mean upwind EC contribution at all supersites was 0.3 μg m^{-3} before the emission adjustment and more than doubled (0.8 μg m^{-3}) after EC emission adjustment. The upwind contribution to the EC concentration at the Baengnyeong supersite was 0.4 μg m^{-3} before the emission adjustment, while it was increased to 0.9 μg m^{-3} after the emission adjustment. The monthly mean downwind contribution to simulated EC concentrations at all supersites was doubled from 0.2 to 0.4 μg m^{-3} after the adjustment (Fig. 8). The monthly mean upwind EC contribution at all supersites, except at the Baengnyeong supersite, was 0.7 μg m^{-3} after EC emission adjustment, showing an increase of 0.4 μg m^{-3} compared with the simulation before the emission adjustment (0.3 μg m^{-3}). Excluding the Baengnyeong supersite, the monthly mean downwind EC contribution averaged over all supersites was 0.3 μg m^{-3} before the emission adjustment, while it increased to 0.5 μg m^{-3} after EC emission adjustment.

The monthly mean upwind EC contribution rate averaged over all supersites increased to 65 % compared to the simulation before the emission adjustment (62 %). Even without considering the Baengnyeong supersite, the monthly mean upwind EC contribution rate averaged over the five supersites increased from 55 % to 59 % after EC emission adjustment. Regardless of the number of supersites, the upwind contribution rate to EC concentrations in the downwind area before and after the EC emission adjustment was over 50 %. Therefore, to reduce EC concentrations in the downwind area, it is critical to not only reduce domestic emissions but also to cooperate with regions in upwind areas. Moreover, even though the downwind EC contribution rate was reduced after emission adjustment, the overall EC emissions were larger after emission adjustment. Therefore, we expect that the required amount of domestic emission reductions based on the emissions inventory should be increased to accomplish the previous goal of EC concentration, such as achieving 30 % of the baseline concentration.

4. Conclusions

In this study, we designed and implemented a two-step emission adjustment approach to improve the reproducibility of air quality modeling to support source-receptor (i.e., upwind-downwind) relationship analysis. Our approach required two steps because traditional emission adjustment with observations assume easy access to observational datasets. Traditional approaches cannot be used when observational data for one region is difficult to acquire. Thus, we designed a new approach where emission adjustment for one region is performed with observations in the other region. Then, a follow-up adjustment for the other region can be done with modeling using updated emissions from the first emission adjustment as well as observational data available for the other region. An objective function based on the described assumption was developed to generate emission adjustment factors by source region. At the same time, to find an optimal solution for the objective function in the form of a matrix, we evaluated three methods: GRGM, PMTRX, and REGF. Based on model performance statistics (NME and correlation coefficient), we selected REGF as the optimal method in this study. The mean errors compared with all supersites and aircraft observational data decreased after the EC emission adjustment with REGF. Also, the NME of the daily mean EC concentration averaged over all supersites decreased from 48 % to 22 %, while the correlation coefficient was maintained at 0.8.

The EC emission adjustment alleviated the underestimation by increasing the simulated EC concentration at the surface and aloft nearly twofold. Therefore, the EC emission adjustment method with REGF is effective when applied with accurate SRR analyses and minimizes the uncertainties of bottom-up emissions inventories by mitigating the time-lag issue of emissions inventories. We used surface and aircraft measurements to examine the utility of the adjusted emissions as surface monitors provide hourly EC data for relatively long periods while aircraft measurements provide higher temporal resolution data and vertical profiles of EC concentrations for a limited number of days.

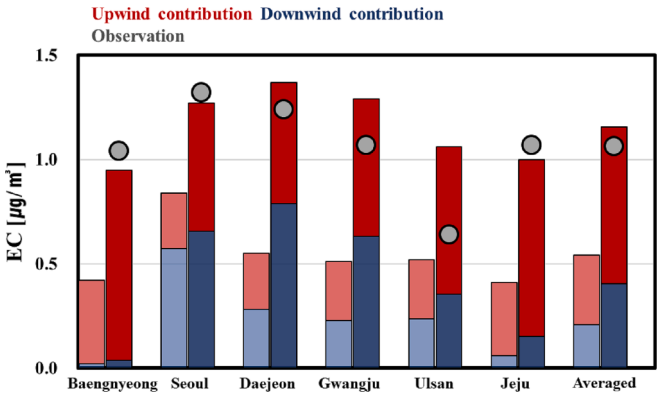

Fig. 8. Upwind (red) and downwind (blue) contributions to the monthly mean elemental carbon (EC) concentrations at the six supersites and averaged across all supersites ("Averaged") in South Korea for May 2016. Lefthand- and righthand-side bars of each paired bar represent the contributions before and after EC emission adjustment, respectively. Grey circles denote the observed EC concentrations. (For interpretation of the references to colour in this figure legend, the reader is referred to the web version of this article.)

After EC emission adjustment with REGF, the upwind and downwind contributions to EC concentrations averaged over all South Korean supersites increased to 0.8 μg m^{-3} (0.3 μg m^{-3} before adjustment) and 0.4 μg m^{-3} (0.2 μg m^{-3} before adjustment), respectively. This is because the EC emission adjusted with REGF increased by 2.5 times compared with that of the emissions inventory in Northeast Asia. Additionally, the upwind contribution rates averaged over all supersites before and after the emission adjustment were 62 % and 65 %, respectively. This implies that the emission adjustment had no significant impact the upwind contribution rate, and the rate was higher than the downwind contribution rate regardless of emission adjustment. Thus, cooperating with regions in upwind areas is essential to improve the EC concentration in South Korea. We demonstrated that our two-step EC emission adjustment approach can provide more accurate estimates of up-to-date emission amounts even if upwind observation points are not readily available, although it would be desirable to secure upwind observational data to utilize more representative upwind contributions for the same approach. Addtionally, we will enhance our monthly-based approach to derive daily/hourly-based emission adjustment in a future study. We expect that the EC emission adjustment method proposed in this study can be successfully used by decision-makers to prepare an integrated air pollution policy.

CRediT authorship contribution statement

Yoon-Hee Kang: Investigation, Visualization, Writing – review & editing. **Kyuwon Son:** Investigation, Visualization, Writing – original draft. **Byeong-Uk Kim:** Methodology, Writing – review & editing. **YuWoon Chang:** Resources. **Hyun Cheol Kim:** Software. **Joshua P. Schwarz:** Resources. **Soontae Kim:** Conceptualization, Writing – review & editing, Supervision.

Declaration of Competing Interest

The authors declare that they have no known competing financial interests or personal relationships that could have appeared to influence the work reported in this paper.

Data availability

Data will be made available on request.

Acknowledgements

Funding: This work was supported by the Korea Ministry of Environment, the National Air Emission Inventory and Research Center and the National Institute of Environmental Research (NIER-2021-04-02-174).

Appendix A. Supplementary material

Supplementary data to this article can be found online at https://doi.org/10.1016/j.envint.2023.108069.

References

Aamaas, B., Bøggild, C.E., Stordal, F., Berntsen, T., Holmèn, K., Ström, J., 2011. Elemental carbon deposition to Svalbard snow from Norwegian settlements and long-range transport. Phys. Meteorol. 63, 340–351. https://doi.org/10.1111/j.1600-0889.2011.00531.x.

Environment Protection Agency (EPA). https://github.com/USEPA/CMAQ/blob/main/CCTM/src/MECHS/saprc07tc_ae6_aq/SpecDef_saprc07tc_ae6_aq.txt (accessed 16 May 2022).

AMS. Air Korea. https://www.airkorea.or.kr (accessed 1 May 2023).

Andreae, M.O., Gelencsér, A., 2006. Black carbon or brown carbon? The nature of light-absorbing carbonaceous aerosols. Atmos. Chem. Phys. 6, 3131–3148. https://doi.org/10.5194/acp-6-3131-2006.

Appel, K.W., Bash, J.O., Fahey, K.M., Foley, K.M., Gilliam, R.C., Hogrefe, C., Hutzell, W. T., Kang, D., Mathur, R., Murphy, B.N., Napelenok, S.L., Nolte, C.G., Pleim, J.E., Pouliot, G.A., Pye, H.O.T., Ran, L., Roselle, S.J., Sarwar, G., Schwede, D.B., Sidi, F.I., Spero, T.L., Wong, D.C., 2021. The community multiscale air quality (CMAQ) model versions 5.3 and 5.3.1: System updates and evaluation. Geosci. Model Dev. 14, 2867–2897. https://doi.org/10.5194/gmd-14-2867-2021.

Bae, H., Lee, S., Jung, D., Oh, G., 2019. Study on the Health Effects of PM2.5 Constituents for Health Risk Reduction Management Plan, Korea Environment Institute.

Bae, C., Kim, H.C., Kim, B.-U., Kim, Y., Woo, J.-H., Kim, S., 2020. Updating Chinese SO_2 emissions with surface observations for regional air-quality modeling over East Asia. Atmos. Environ. 228, 117416 https://doi.org/10.1016/j.atmosenv.2020.117416.

Bae, M., Kim, E., You, S., Son, K., Kang, Y.-H., Kim, S.T., 2021. Local authority level source apportionments of $PM_{2.5}$ concentrations based on the CAPSS 2016: (VII) Seoul. J. Korean Soc. Atmos. Environ. 37, 466–486. https://doi.org/10.5572/KOSAE.2021.37.3.466.

Binkowski, F.S., 1999. Aerosols in Models-3 CMAQ. In: Byun, D. (Ed.), Science Algorithms of the EPA Models-3 community multiscale air quality (CMAQ) Modeling System, EPA/600/R-99/030. Office of Research and Development, Unites States Environmental Protection Agency, Washington, pp. 10–11.

Binkowski, F.S., Roselle, S.J., 2003. Models-3 community multiscale air quality (CMAQ) model aerosol component 1. Model description. J. Geophys. Res. 108, 4183. https://doi.org/10.1029/2001JD001409.

Blanchard, C.L., Shaw, S.L., Edgerton, E.S., Schwab, J.J., 2019. Emission influences on air pollutant concentrations in New York state: II. $PM_{2.5}$ organic and elemental carbon constituents. Atmos. Environ. X. 3, 100039. https://doi.org/10.1016/j.aeaoa.2019.100039.

Byun, D., Schere, K.L., 2006. Review of the governing equations, computational algorithms, and other components of the models-3 community multiscale air quality (CMAQ) modeling system. Appl. Mech. Rev. 59, 51–77. https://doi.org/10.1115/1.2128636.

Carter, W.P.L., 2010. Development of the SAPRC-07 chemical mechanism. Atmos. Environ. 44, 5324–5335. https://doi.org/10.1016/j.atmosenv.2010.01.026.

National Centers for Environmental Prediction (NCEP), Ncep, F.N.L., 2000. Operational Model Global Tropospheric Analyses, Continuing from July 1999, Research Data Archive at the National Center for Atmospheric Research. Computational and Information Systems Laboratory.

MADIS. NCEP Central Operations. https://madis.ncep.noaa.gov (accessed 1 May 2023).

Chai, H., Kang, B., Kim, J.-S., Moon, J., Kim, J.-C., 2015. Study of drawing optimum switch automation rate to minimize reliability cost. Trans. Korean Inst. Electr. Eng. 64, 297–302. https://doi.org/10.5370/KIEEP.2015.64.4.297.

Chatani, S., Morino, Y., Shimadera, H., Hayami, H., Mori, Y., Sasaki, K., Kajino, M., Yokoi, T., Morikawa, T., Ohara, T., 2014. Multi-model analyses of dominant factors influencing elemental carbon in Tokyo metropolitan area of Japan. Aerosol Air Qual. Res. 14, 396–405. https://doi.org/10.4209/aaqr.2013.02.0035.

Chatani, S., Yamaji, K., Sakurai, T., Itahashi, S., Shimadera, H., Kitayama, K., Hayami, H., 2018. Overview of model inter- comparison in Japan's Study for reference air quality modeling (J-STREAM). Atmosphere. 9, 19. https://doi.org/10.3390/atmos9010019.

Chen, G., Guan, Y., Tong, L., Yan, B., Hou, L., 2015. Spatial estimation of $PM_{2.5}$ emissions from straw open burning in Tianjin from 2001 to 2012. Atmos. Environ. 122, 705–712. https://doi.org/10.1016/j.atmosenv.2015.10.043.

Cheng, Z., Luo, L., Wang, S., Wang, Y., Sharma, S., Shimadera, H., Wang, X., Bressi, M., de Miranda, R.M., Jiang, J., Zhou, W., Fajardo, O., Yan, N., Hao, J., 2016. Status and characteristics of ambient $PM_{2.5}$ pollution in global megacities. Environ. Int. 89–90, 212–221. https://doi.org/10.1016/j.envint.2016.02.003.

Cheng, L., Ye, Z., Cheng, S., Guo, X., 2021. Agricultural ammonia emissions and its impact on $PM_{2.5}$ concentrations in the Beijing–Tianjin–Hebei region from 2000 to 2018. Environ. Pollut. 291, 118162 https://doi.org/10.1016/j.envpol.2021.118162.

Cho, H.-J., Jang, S.-H., Kim, Y.-S., 2008. Development of CO_2 emission estimation model by multiple regression analysis. Korean J. Environ. Health Sci. 34, 316–326. https://doi.org/10.5668/JEHS.2008.34.4.316.

Cho, C., Schwarz, J.P., Perring, A.E., Lamb, K.D., Kondo, Y., Park, J.U., Park, D.H., Shim, K., Park, J.S., Park, R.J., Lee, M., Song, C.K., Kim, S.W., 2021. Light-absorption enhancement of black carbon in the Asian outflow inferred from airborne SP2 and in-situ measurements during KORUS-AQ. Sci. Total Environ. 773, 145531 https://doi.org/10.1016/j.scitotenv.2021.145531.

Choi, S., Kim, T., Lee, H., Kim, H., Han, J., Lee, K., Lim, E., Shin, S., Jin, H., Cho, E., Kim, Y., Yoo, C., 2020. Analysis of the national air pollutant emission inventory (CAPSS 2016) and the major cause of change in Republic of Korea. Asian J. Atmos. Environ. 14, 422–445. https://doi.org/10.5572/ajae.2020.14.4.422.

Crawford, J.H., Ahn, J.-Y., Al-Saadi, J., Chang, L., Emmons, L.K., Kim, J., Lee, G., Park, J.-H., Park, R.J., Woo, J.H., Song, C.-K., Hong, J.-H., Hong, Y.-D., Lefer, B.L., Lee, M., Lee, T., Kim, S., Min, K.-E., Yum, S.S., Shin, H.J., Kim, Y.-W., Choi, J.-S., Park, J.-S., Szykman, J.J., Long, R.W., Jordan, C.E., Simpson, I.J., Fried, A., Dibb, J.E., Cho, S., Kim, Y.P. 2021. The Korea–United States Air Quality (KORUS-AQ) field study. Elementa: Sci. Anthropocene 9, 00163. https://doi.org/10.1525/elementa.2020.00163.

Choi, J., Park, R.J., Lee, H.-M., Lee, S., Jo, D.S., Jeong, J.I., Henze, D.K., Woo, J.-H., Ban, S.-J., Lee, M.-D., Lim, C.-S., Park, M.-K., Shin, H.J., Cho, S., Peterson, D., Song, C.-K., 2019. Impacts of local vs. trans-boundary emissions from different sectors on $PM_{2.5}$ exposure in South Korea during the KORUS-AQ campaign. Atmos. Environ. 203, 196–205. https://doi.org/10.1016/j.atmosenv.2019.02.008.

Dauda, J.A., Rahmon, S.A., Tijani, I.A., Mohammad, F., Okegbenro, W.O., 2022. Design optimization of reinforced concrete pile foundation using generalized reduced gradient algorithm. Front. Eng. Built Environ. 2, 133–153. https://doi.org/10.1108/febe-12-2021-0059.

Emery, C., Tai, E., Yarwood, G., 2001. Enhanced meteorological modeling and performance evaluation for two Texas ozone episodes, Prepared for the Texas Natural Resource Conservation Commission, by ENVIRON International Corporation, 161.

Emery, C., Liu, Z., Russell, A.G., Odman, M.T., Yarwood, G., Kumar, N., 2017. Recommendations on statistics and benchmarks to assess photochemical model performance. J. Air Waste Manag. Assoc. 67, 582–598. https://doi.org/10.1080/10962247.2016.1265027.

Fiore, A.M., Dentener, F.J., Wild, O., Cuvelier, C., Schultz, M.G., Hess, P., Textor, C., Schulz, M., Doherty, R.M., Horowitz, L.W., MacKenzie, I.A., Sanderson, M.G., Shindell, D.T., Stevenson, D.S., Szopa, S., Van Dingenen, R., Zeng, G., Atherton, C., Bergmann, D., Bey, I., Carmichael, G., Collins, W.J., Duncan, B.N., Faluvegi, G., Folberth, G., Gauss, M., Gong, S., Hauglustaine, D., Holloway, T., Isaksen, I.S.A., Jacob, D.J., Jonson, J.E., Kaminski, J.W., Keating, T.J., Lupu, A., Marmer, E., Montanaro, V., Park, R.J., Pitari, G., Pringle, K.J., Pyle, J.A., Schroeder, S., Vivanco, M.G., Wind, P., Wojcik, G., Wu, S., Zuber, A., 2009. Multimodel estimates of intercontinental source-receptor relationships for ozone pollution. J. Geophys. Res. 114, 4301. https://doi.org/10.1029/2008JD010816.

Fisher, B.E.A., Sokhi, R.S., 2000. Investigation of roadside concentrations in busy streets using the model GRAM: Conditions leading to high short-term concentrations. Int. J. Environ. Pollut. 14, 488. https://doi.org/10.1504/IJEP.2000.000572.

Fowler, D., Muller, J., Smith, R.I., Cape, J.N., Erisman, J.W., 2005. Nonlinearities in Source Receptor Relationships for sulfur and nitrogen compounds. AMBIO J. Hum. Environ. 34, 41–46. https://doi.org/10.1579/0044-7447-34.1.41.

Frey, H.C., Zheng, J., 2002. Quantification of variability and uncertainty in air pollutant emission inventories: method and case study for utility NOx emissions. J. Air Waste Manage. Assoc. 52, 1083–1095. https://doi.org/10.1080/10473289.2002.10470837.

Geem, Z.W., Geem, W.B., 2007. Cutting-edge optimization technique and its applications to the civil engineering. Mag. Korean Soc. Civil Eng. 55, 155–171.

Ensberg, J.J., Craven, J.S., Metcalf, A.R., Allan, J.D., Angevine, W.M., Bahreini, R., Brioude, J., Cai, C., Coe, H., de Gouw, J.A., Ellis, R.A., Flynn, J.H., Haman, C.L., Hayes, P.L., Jimenez, J.L., Lefer, B.L., Middlebrook, A.M., Murphy, J.G., Neuman, J. A., Nowak, J.B., Roberts, J.M., Stutz, J., Taylor, J.W., Veres, P.R., Walker, J.M., Seinfeld, J.H., 2013. Inorganic and black carbon aerosols in the Los Angeles Basin during CalNex:. J. Geophys. Res. Atmos. 118, 1777–1803. https://doi.org/10.1029/2012JD018136, 2013.

He, Z., Kim, Y.J., Ogunjobi, K.O., Kim, J.E., Ryu, S.Y., 2004. Carbonaceous aerosol characteristics of $PM_{2.5}$ particles in northeastern Asia in summer 2002. Atmos. Environ. 38, 1795–1800. https://doi.org/10.1016/j.atmosenv.2003.12.023.

Heintzenberg, J., Winkler, P., 1991. Elemental carbon in the atmosphere: Challenges for the trace analyst. Fresenius J. Anal. Chem. 340, 540–543. https://doi.org/10.1007/BF00322425.

Houyoux, M.R., Vukovich, J.M., Coats Jr, J.C., Wheeler, N.J.M., Kasibhatla, P.S., 2000. Emission inventory development and processing for the seasonal model for regional air quality (SMRAQ) project. J. Geophys. Res. 105, 9079–9090. https://doi.org/10.1029/1999JD900975.

Hu, Y., Napelenok, S.L., Odman, M.T., Russell, A.G., 2009a. Sensitivity of inverse estimation of 2004 elemental carbon emissions inventory in the United States to the choice of observational networks. Geophys. Res. Lett. 36, L15806. https://doi.org/10.1029/2009GL039655.

Hu, Y., Odman, M.T., Russell, A.G., 2009b. Top-down analysis of the elemental carbon emissions inventory in the United States by inverse modeling using Community Multiscale Air Quality model with decoupled direct method (CMAQ-DDM). J. Geophys. Res. 114, D24. https://doi.org/10.1029/2009JD011987.

National Geographic Information Institute (NGII), 2022. http://map.ngii.go.kr/ms/map/NlipMap.do?tabGb=statsMap (accessed 14 March 2020).

IARC Working Group on the Evaluation of Carcinogenic Risks to Humans, 2016. Outdoor Air Pollution. IARC monographs on the evaluation of carcinogenic risks to humans 109, 9–444.
Jang, Y., Lee, Y., Kim, J., Kim, Y., Woo, J.-H., 2020. Improvement China point source for improving bottom-up emission inventory. Asia-Pac. J. Atmos. Sci. 56, 107–118. https://doi.org/10.1007/s13143-019-00115-y.
Janssen, N.A.H., Hoek, G., Simic-Lawson, M., Fischer, P., van Bree, L., ten Brink, H., Keuken, M., Atkinson, R.W., Anderson, H.R., Brunekreef, B., Cassee, F.R., 2011. Black Carbon as an Additional Indicator of the Adverse Health Effects of Airborne Particles Compared with PM_{10} and $PM_{2.5}$. Environ. Health Perspect. 119, 1691–1699. https://doi.org/10.1289/ehp.1003369.
Jeong, S.-Y., Kim, C.-H., 2021. Bias analysis of WRF-CMAQ simulated PM2.5 concentrations caused by different PBL parameterizations: Application to the haze period of march in 2019 over the Seoul metropolitan area. J. Korean Soc. Atmos. Environ. 37, 835–852. https://doi.org/10.5572/KOSAE.2021.37.6.835.
Jo, Y.-J., Lee, H.-J., Jo, H.-Y., Woo, J.-H., Kim, Y., Lee, T., Heo, G., Park, S.-M., Jung, D., Park, J., Kim, C.-H., 2020. Changes in inorganic aerosol compositions over the Yellow Sea area from impact of Chinese emissions mitigation. Atmos. Res. 240, 104948 https://doi.org/10.1016/j.atmosres.2020.104948.
Jorquera, H., Castro, J., 2010. Analysis of urban pollution episodes by inverse modeling. Atmos. Environ. 44, 42–54. https://doi.org/10.1016/j.atmosenv.2009.09.040.
Kang, C.-M., Kang, B.-W., Lee, H.S., 2006. Source identification and trends in concentrations of gaseous and fine particulate principal species in Seoul, South Korea. J. Air Waste Manage. Assoc. 56, 911–921. https://doi.org/10.1080/10473289.2006.10464506.
Khan, A.J., Li, J., Husain, L., 2006. Atmospheric transport of elemental carbon. J. Geophys. Res. 111, D04303. https://doi.org/10.1029/2005JD006505.
Kiesewetter, G., Borken-Kleefeld, J., Schöpp, W., Heyes, C., Bertok, I., Thunis, P., Bessagnet, B., Terrenoire, E., Amann, M., 2013. Modelling Compliance with NO_2 and PM_{10} Air Quality Limit Values in the GAINS Model, TSAP Report 9. DG Environment of the European Commission, Belgium.
Kim, Y.P., 2000. Organic and elemental carbon in fine particles at Kosan. Korea. Atmos. Environ. 34, 3309–3317. https://doi.org/10.1016/S1352-2310(99)00445-8.
Kim, H.C., Bae, C., Bae, M., Kim, O., Kim, B.-U., Yoo, C., Park, J., Choi, J., Lee, J., Lefer, B., Stein, A., Kim, S., 2020. Space-borne monitoring of NOx emissions from cement kilns in South Korea. Atmosphere. 11, 881. https://doi.org/10.3390/atmos11080881.
Kim, N.K., Kim, Y.P., Morino, Y., Kurokawa, J., Ohara, T., 2014. Verification of NOx emission inventories over North Korea. Environ. Pollut. 195, 236–244. https://doi.org/10.1016/j.envpol.2014.06.034.
Kim, B.-U., Kim, H.C., Kim, S., 2021a. Effects of vertical turbulent diffusivity on regional $PM_{2.5}$ and O_3 source contributions. Atmos. Environ. 245, 118026 https://doi.org/10.1016/j.atmosenv.2020.118026.
Kim, B.-G., Moon, Y.-T., Kim, H.-S., Kim, J.-R., 2007. Forecast of influent characteristics in wastewater treatment plant with time series model. J. Korean Soc. Water Wastewater. 21, 701–707.
Kim, S., You, S., Kang, Y.-H., Kim, E., Bae, M., Son, K., Kim, Y., Kim, B.-U., Kim, H.C., 2021b. Municipality-level source apportionment of $PM_{2.5}$ concentrations based on the CAPSS 2016: (II) Incheon. J. Korean Soc. Atmos. Environ. 37, 144–168. https://doi.org/10.5572/KOSAE.2021.37.1.144.
Kim, S., You, S., Kim, E., Kang, Y.-H., Bae, M., Son, K., 2021c. Municipality-level source apportionment of $PM_{2.5}$ concentrations based on the CAPSS 2016: (III) Jeollanamdo. J. Korean Soc. Atmos. Environ. 37, 206–230. https://doi.org/10.5572/KOSAE.2021.37.2.206.
Kondo, Y., Komazaki, Y., Miyazaki, Y., Moteki, N., Takegawa, N., Kodama, D., Deguchi, S., Nogami, M., Fukuda, M., Miyakawa, T., Morino, Y., Koike, M., Sakurai, H., Ehara, K., 2006. Temporal variations of elemental carbon in Tokyo. J. Geophys. Res. 111, D12205. https://doi.org/10.1029/2005JD006257.
Krall, J.R., Anderson, G.B., Dominici, F., Bell, M.L., Peng, R.D., 2013. Short-term exposure to particulate matter constituents and mortality in a national study of U.S. Urban communities. Environ. Health Perspect. 121, 1148–1153. https://doi.org/10.1289/ehp.1206185.
Kublanovskaya, V.N., 1966. Evaluation of a generalized inverse matrix and projector. USSR Comp. Math. Math. Phys. 6, 179–188. https://doi.org/10.1016/0041-5553(66)90064-4.
Kurokawa, J., Ohara, T., 2020. Long-term historical trends in air pollutant emissions in Asia: Regional Emission inventory in ASia (REAS) version 3. Atmos. Chem. Phys. 20, 12761–12793. https://doi.org/10.5194/acp-20-12761-2020.
L3HARRIS, 2022. https://www.l3harrisgeospatial.com/docs/regress.html (accessed on 6 Apr 2022).
Lamb, K.D., Perring, A.E., Samset, B., Peterson, D., Davis, S., Anderson, B.E., Beyersdorf, A., Blake, D.R., Campuzano-Jost, P., Corr, C.A., Diskin, G.S., Kondo, Y., Moteki, N., Nault, B.A., Oh, J., Park, M., Pusede, S.E., Simpson, I.J., Thornhill, K.L., Wisthaler, A., Schwarz, J.P., 2018. Estimating source region influences on black carbon abundance, microphysics, and radiative effect observed over South Korea. J. Geophys. Res. Atmospheres. 123, 13527–13548. https://doi.org/10.1029/2018JD029257.
Lan, Z., Zhang, B., Huang, X., Zhu, Q., Yuan, J., Zeng, L., Hu, M., He, L., 2018. Source apportionment of $PM_{2.5}$ light extinction in an urban atmosphere in China. J. Environ. Sci. (China) 63, 277–284. https://doi.org/10.1016/j.jes.2017.07.016.
Lee, T., Choi, J., Lee, G., Ahn, J., Park, J.S., Atwood, S.A., Schurman, M., Choi, Y., Chung, Y., Collett, J.L., 2015b. Characterization of aerosol composition, concentrations, and sources at Baengnyeong Island, Korea using an aerosol mass spectrometer. Atmos. Environ. 120, 297–306. https://doi.org/10.1016/j.atmosenv.2015.08.038.
Lee, D., Choi, J.-Y., Myoung, J., Kim, O., Park, J., Shin, H.-J., Ban, S.-J., Park, H.-J., Nam, K.-P., 2019. Analysis of a severe $PM_{2.5}$ episode in the Seoul metropolitan area in South Korea from 27 February to 7 March 2019: Focused on estimation of domestic and foreign contribution. Atmosphere. 10, 756. https://doi.org/10.3390/atmos10120756.
Lee, H.J., Jo, H.Y., Kim, S.W., Park, M.S., Kim, C.H., 2019b. Impacts of atmospheric vertical structures on transboundary aerosol transport from China to South Korea. Sci. Rep. 9, 13040. https://doi.org/10.1038/s41598-019-49691-z.
Lee, H.-J., Jo, H.-Y., Song, C.-K., Jo, Y.-J., Park, S.-Y., Kim, C.-H., 2020. Sensitivity of simulated PM2.5 concentrations over Northeast Asia to different secondary organic aerosol modules during the KORUS-AQ campaign. Atmosphere. 11, 1004. https://doi.org/10.3390/atmos11091004.
Lee, K., Kim, Y.J., Kang, C.-H., Kim, J.-S., Park, K., 2015a. Chemical characteristics of long-range-transported fine particulate matter at Gosan, Jeju Island. J. Air Waste Manage. Assoc. 65, 445–454. https://doi.org/10.1080/10962247.2014.1001883.
Lee, S.-G., Kim, J.-H., Kim, S.-S., 2017. A case study of exposure to elemental carbon (EC) in an underground copper ore mine. J. Environ. Sci. Int. 26, 1013–1021. https://doi.org/10.5322/JESI.2017.26.9.1013.
Li, K., Liao, H., Mao, Y., Ridley, D.A., 2016. Source sector and region contributions to concentration and direct radiative forcing of black carbon in China. Atmos. Environ. 124, 351–366. https://doi.org/10.1016/j.atmosenv.2015.06.014.
Lu, M., Tang, X., Wang, Z., Wu, L., Chen, X., Liang, S., Zhou, H., Wu, H., Hu, K., Shen, L., Yu, J., Zhu, J., 2019. Investigating the transport mechanism of $PM_{2.5}$ pollution during January 2014 in Wuhan. Central China. Adv. Atmos. Sci. 36, 1217–1234. https://doi.org/10.1007/s00376-019-8260-5.
Luo, X., Tang, X., Wang, H., Kong, L., Wu, H., Wang, W., Song, Y., Luo, H., Wang, Y., Zhu, J., Wang, Z., 2023. Investigating the changes in air pollutant emissions over the Beijing-Tianjin-Hebei region in February from 2014 to 2019 through an inverse emission method. Adv. Atmos. Sci. 40, 601–618. https://doi.org/10.1007/s00376-022-2039-9.
Mao, Q., Gautney, L.L., Cook, T.M., Jacobs, M.E., Smith, S.N., Kelsoe, J.J., 2006. Numerical experiments on MM5–CMAQ sensitivity to various PBL schemes. Atmos. Environ. 40, 3092–3110. https://doi.org/10.1016/j.atmosenv.2005.12.055.
Matveev, A.A., 1974. An algorithm for the pseudoinversion of matrices. USSR Comp. Math. Math. Phys. 14, 208–212. https://doi.org/10.1016/0041-5553(74)90053-6.
Moon, N., Kim, S., Seo, J., 2011. Sensibility study for PBL scheme of WRF-CMAQ. J. Korean Soc. Atmos. Environ. 27, 791–804. https://doi.org/10.5572/KOSAE.2011.27.6.791.
Morawska, L., Hofmann, W., Hitchins-Loveday, J., Swanson, C., Mengersen, K., 2005. Experimental study of the deposition of combustion aerosols in the human respiratory tract. J. Aerosol Sci. 36, 939–957. https://doi.org/10.1016/j.jaerosci.2005.03.015.
NAAQMN. China National Environmental Monitoring Centre. https://www.cnemc.cn/en (accessed 1 May 2023).
NIER (National Institute of Environmental Research), 2017. KORUS-AQ Rapid Science Synthesis Report. Incheon: NIER.
Ogren, J.A., Charlson, R.J., 1984. Wet deposition of elemental carbon and sulfate in Sweden. Tellus B. 36B, 262–271. https://doi.org/10.1111/j.1600-0889.1984.tb00246.x.
Park, S.S., Cho, S.Y., 2011. Tracking sources and behaviors of water-soluble organic carbon in fine particulate matter measured at an urban site in Korea. Atmos. Environ. 45, 60–72. https://doi.org/10.1016/j.atmosenv.2010.09.045.
Peterson, D.A., Hyer, E.J., Han, S.-O., Crawford, J.H., Park, R.J., Holz, R., Kuehn, R.E., Eloranta, E., Knote, C., Jordan, C.E., Lefer, B.L., 2019. Meteorology influencing springtime air quality, pollution transport, and visibility in Korea. Elem. Sci. Anthropocene. 7, 57. https://doi.org/10.1525/elementa.395.
Petzold, A., Ogren, J.A., Fiebig, M., Laj, P., Li, S.-M., Baltensperger, U., Holzer-Popp, T., Kinne, S., Pappalardo, G., Sugimoto, N., Wehrli, C., Wiedensohler, A., Zhang, X.-Y., 2013. Recommendations for reporting black carbon measurements. Atmos. Chem. Phys. 13, 8365–8379. https://doi.org/10.5194/acp-13-8365-2013.
Qiu, X., Duan, L., Gao, J., Wang, S., Chai, F., Hu, J., Zhang, J., Yun, Y., 2016. Chemical composition and source apportionment of PM_{10} and $PM_{2.5}$ in different functional areas of Lanzhou. China. J. Environ. Sci. (China) 40, 75–83. https://doi.org/10.1016/j.jes.2015.10.021.
Rappazzo, K.M., Daniels, J.L., Messer, L.C., Poole, C., Lobdell, D.T., 2015. Exposure to elemental carbon, organic carbon, nitrate, and sulfate fractions of fine particulate matter and risk of preterm birth in New Jersey, Ohio, and Pennsylvania (2000–2005). Environ. Health Perspect. 123, 1059–1065. https://doi.org/10.1289/ehp.1408953.
Rissman, J., Arunachalam, S., Woody, M., West, J.J., BenDor, T., Binkowski, F.S., 2013. A plume-in-grid approach to characterize air quality impacts of aircraft emissions at the Hartsfield-Jackson Atlanta International Airport. Atmos. Chem. Phys. 13, 9285–9302. https://doi.org/10.5194/acp-13-9285-2013.
Shu, Q., Koo, B., Yarwood, G., Henderson, B.H., 2017. Strong influence of deposition and vertical mixing on secondary organic aerosol concentrations in CMAQ and CAMx. Atmos. Environ. 171, 317–329. https://doi.org/10.1016/j.atmosenv.2017.10.035.
Shu, Y., Lam, N.S.N., 2011. Spatial disaggregation of carbon dioxide emissions from road traffic based on multiple linear regression model. Atmos. Environ. 45, 634–640. https://doi.org/10.1016/j.atmosenv.2010.10.037.
Skamarock, W.C., Klemp, J.B., 2008. A time-split nonhydrostatic atmospheric model for weather research and forecasting applications. J. Comp. Phys. 227, 3465–3485. https://doi.org/10.1016/j.jcp.2007.01.037.
So, Y.-Y., Song, S.-K., Choi, Y.-N., 2019. Comparison of the concentration characteristics and optical properties of aerosol chemical components in different regions. J. Environ. Sci. Int. 28, 107–123. https://doi.org/10.5322/JESI.2019.28.1.107.

Stavrakou, T., Müller, J.-F., Boersma, K.F., van der A, R.J., Kurokawa, J., Ohara, T., Zhang, Q., 2013. Key chemical NO_x sink uncertainties and how they influence top-down emissions of nitrogen oxides. Atmos. Chem. Phys. 13, 9057–9082. https://doi.org/10.5194/acp-13-9057-2013.

Su, W., Liu, Y., Wang, S., Zhao, Y., Su, Y., Li, S., 2018. Regional inequality, spatial spillover effects, and the factors influencing city-level energy-related carbon emissions in China. J. Geogr. Sci. 28, 495–513. https://doi.org/10.1007/s11442-018-1486-9.

Sung, M., Moon, K., Park, J., Kim, H., Jeon, H., Choi, J., Ahn, J., Hong, Y., 2017. Chemical composition and source apportionment using the PMF model of the ambient $PM_{2.5}$ in 2013 over Korea. J. Korean Soc. Urban Environ. 17, 145–156.

Tang, W., Emmons, L.K., Arellano Jr, A.F., Gaubert, B., Knote, C., Tilmes, S., Buchholz, R. R., Pfister, G.G., Diskin, G.S., Blake, D.R., Blake, N.J., Meinardi, S., DiGangi, J.P., Choi, Y., Woo, J.-H., He, C., Schroeder, J.R., Suh, I., Lee, H., Jo, H., Kanaya, Y., Jung, J., Lee, Y., Kim, D., 2019. Source contributions to carbon monoxide concentrations during KORUS-AQ based on CAM-chem model applications. J. Geophys. Res. Atmospheres. 124, 2796–2822. https://doi.org/10.1029/2018JD029151.

Travis, K.R., Crawford, J.H., Chen, G., Jordan, C.E., Nault, B.A., Kim, H., Jimenez, J.L., Campuzano-Jost, P., Dibb, J.E., Woo, J.-H., Kim, Y., Zhai, S., Wang, X., McDuffie, E. E., Luo, G., Yu, F., Kim, S., Simpson, I.J., Blake, D.R., Chang, L., Kim, M.J., 2022. Limitations in representation of physical processes prevent successful simulation of PM2.5 during KORUS-AQ. Atmos. Chem Phys. 22, 7933–7958. https://doi.org/10.5194/acp-22-7933-2022.

Uno, I., Wang, Z., Itahashi, S., Yumimoto, K., Yamamura, Y., Yoshino, A., Takami, A., Hayasaki, M., Kim, B.G., 2020. Paradigm shift in aerosol chemical composition over regions downwind of China. Sci. Rep 10, 6450. https://doi.org/10.1038/s41598-020-63592-6.

Viana, M., Maenhaut, W., ten Brink, H.M., Chi, X., Weijers, E., Querol, X., Alastuey, A., Mikuška, P., Večeřa, Z., 2007. Comparative analysis of organic and elemental carbon concentrations in carbonaceous aerosols in three European cities. Atmos. Environ. 41, 5972–5983. https://doi.org/10.1016/j.atmosenv.2007.03.035.

Wagstrom, K.M., Pandis, S.N., 2011. Source–receptor relationships for fine particulate matter concentrations in the Eastern United States. Atmos. Environ. 45, 347–356. https://doi.org/10.1016/j.atmosenv.2010.10.019.

Wang, Y., Li, L., Chen, C., Huang, C., Huang, H., Feng, J., Wang, S., Wang, H., Zhang, G., Zhou, M., Cheng, P., Wu, M., Sheng, G., Fu, J., Hu, Y., Russell, A.G., Wumaer, A., 2014. Source apportionment of fine particulate matter during autumn haze episodes in Shanghai. China. J. Geophys. Res. Atmos. 119, 1903–1914. https://doi.org/10.1002/2013JD019630.

Wang, P., Wang, H., Wang, Y.Q., Zhang, X.Y., Gong, S.L., Xue, M., Zhou, C.H., Liu, H.L., An, X.Q., Niu, T., Cheng, Y.L., 2016b. Inverse modeling of black carbon emissions over China using ensemble data assimilation. Atmos. Chem. Phys. 16, 989–1002. https://doi.org/10.5194/acp-16-989-2016.

Wang, J., Xu, J., He, Y., Chen, Y., Meng, F., 2016a. Long range transport of nitrate in the low atmosphere over NorthEast Asia. Atmos. Environ. 144, 315–324. https://doi.org/10.1016/j.atmosenv.2016.08.084.

Wolff, G.T., 1981. Particulate elemental carbon in the atmosphere. J. Air Pollut. Control Assoc. 31, 935–938. https://doi.org/10.1080/00022470.1981.10465298.

Xing, L., Li, G., Pongpiachan, S., Wang, Q., Han, Y., Cao, J., Tipmanee, D., Palakun, J., Aukkaravittayapun, S., Surapipith, V., Poshyachinda, S., 2020. Quantifying the contributions of local emissions and regional transport to elemental carbon in Thailand. Environ. Pollut. 262, 114272 https://doi.org/10.1016/j.envpol.2020.114272.

Yamagami, M., Ikemori, F., Nakashima, H., Hisatsune, K., Osada, K., 2019. Decreasing trend of elemental carbon concentration with changes in major sources at Mega city Nagoya, Central Japan. Atmos. Environ. 199, 155–163. https://doi.org/10.1016/j.atmosenv.2018.11.014.

You, S., Kang, Y.-H., Kim, B.-U., Kim, H.C., Kim, S., 2021. The role of a distant typhoon in extending a high $PM_{2.5}$ episode over Northeast Asia. Atmos. Environ. 257, 118480 https://doi.org/10.1016/j.atmosenv.2021.118480.

Yu, S., Dennis, R.L., Bhave, P.V., Eder, B.K., 2004. Primary and secondary organic aerosols over the United States: Estimates on the basis of observed organic carbon (OC) and elemental carbon (EC), and air quality modeled primary OC/EC ratios. Atmos. Environ. 38, 5257–5268. https://doi.org/10.1016/j.atmosenv.2004.02.064.

Yu, Z., Jang, M., Kim, S., Bae, C., Koo, B., Beardsley, R., Park, J., Chang, L.S., Lee, H.C., Lim, Y.-K., Cho, J.H., 2020. Simulating the impact of long-range-transported Asian mineral dust on the formation of sulfate and nitrate during the KORUS-AQ campaign. ACS Earth Space Chem. 4, 1039–1049. https://doi.org/10.1021/acsearthspacechem.0c00074.

Zhang, L., Chen, Y., Zhao, Y., Henze, D.K., Zhu, L., Song, Y., Paulot, F., Liu, X., Pan, Y., Lin, Y., Huang, B., 2018. Agricultural ammonia emissions in China: Reconciling bottom-up and top-down estimates. Atmos. Chem. Phys. 18, 339–355. https://doi.org/10.5194/acp-18-339-2018.

Zhang, Q., Xue, D., Liu, X., Gong, X., Gao, H., 2019. Process analysis of PM2.5 pollution events in a coastal city of China using CMAQ. J. Environ. Sci. (China) 79, 225–238. https://doi.org/10.1016/j.jes.2018.09.007.

Zhao, Y., Nielsen, C.P., Lei, Y., McElroy, M.B., Hao, J., 2011. Quantifying the uncertainties of a bottom-up emission inventory of anthropogenic atmospheric pollutants in China. Atmos. Chem. Phys. 11, 2295–2308. https://doi.org/10.5194/acp-11-2295-2011.